Magnetically tunable exciton valley coherence in monolayer WS_2 mediated by the electron-hole exchange and exciton-phonon interactions

Kang Lan [1], Shijie Xie [1,*], Jiyong Fu [2,†] and Fanyao Qu [3]

[1] *School of Physics, State Key Laboratory of Crystal Materials, Shandong University, Jinan 250100, China*

[2] *Department of Physics, Qufu Normal University, Qufu 273165, China*

[3] *Instituto de Física, Universidade de Brasília, Brasília-DF 70919-970, Brazil*

(Received 25 November 2022; revised 28 May 2023; accepted 10 July 2023; published 26 July 2023)

We develop a model which incorporates both intra- and intervalley scatterings to master equation, to explore exciton valley coherence in monolayer WS_2 subjected to magnetic field. For linearly polarized (LP) excitation accompanied with an *initial* coherence, our determined valley dynamics manifests the coherence decay being faster than the exciton population relaxation and agrees with experimental data by Hao *et al.* [Nat. Phys. **12**, 677 (2016)]. Further, we reveal that magnetic field may quench the electron-hole (e-h) exchange-induced pure dephasing—a crucial decoherence source—as a result of lifting of valley degeneracy, allowing one to *magnetically* regulate valley coherence. In particular, at low temperatures for which the exciton-phonon (ex-ph) interaction is weak, we find that the coherence time is expected to attain $\tau_C \sim 1$ ps, facilitating full control of qubits based on the valley pseudospin. For dark excitons, we demonstrate an emerging coherence even in the absence of initial coherent state, which has a long coherence time (∼15 ps) at low temperature. Our work provides an insight into *tunable* valley coherence and coherent valley control based on dark excitons.

DOI: 10.1103/PhysRevB.108.035419

I. INTRODUCTION

Among emerging new two-dimensional materials utilized for valleytronic applications [1], monolayer transition-metal dichalcogenides (TMDCs) MX_2 (M = Mo, W; X = S, Se, Te) have attracted intense research interest following the discovery of a direct band gap at the two inequivalent K and K' valleys of the Brillouin zone [2]. Owing to the reduced dielectric screening and large electron (and hole) effective masses, the light-matter interaction in TMDCs is dominated by tightly Coulomb-bound excitons with the binding energy up to hundreds of meV [3,4]. Also, the space inversion asymmetry together with spin-orbit interaction endows TMDCs the spin-valley *locked* band structure [2,5,6], which enables optical generation and manipulation of valley polarization, as well as extraction of valley pseudospin information with the aid of circularly polarized (CP) light [7–12], and facilitates control of valley coherence of excitons.

Benefiting from the valley selective transition rule [2], the initial coherent state for excitons is typically generated *via* optical pumping of linearly polarized (LP) light [13–19]. And, the control of valley coherence, which features a rotation of polarized light emission (referring to a rotation of coherent superposition of valley exciton states), has widely been reported by resorting to magnetic field [20,21]. Further, both the direction and speed of coherent rotation can be manipulated by tuning the dynamic phase of excitons hosted in distinct valleys [22]. However, despite substantial efforts, so far a fundamental microscopic model describing the dynamical evolution of valley (exciton) coherence in TMDCs from which the coherence intensity and time—crucial quantities for valley manipulation—can be directly inferred, is still not available, though is greatly desired from both fundamental physics and experimental application points of view.

Here we develop a model for valley exciton dynamics in monolayer WS_2 subjected to magnetic field, by incorporating both intra- and intervalley scatterings associated with the exciton recombination, electron-hole (e-h) exchange, and exciton-phonon (ex-ph) interactions, to master equation. We then determine how the valley coherence evolves with time and further unveil the potential means of how to enhance it in practice. In addition to the LP excitation, which is widely adopted in experiments for coherent valley control [20,21], we also demonstrate an emerging valley coherence of dark excitons even in the absence of initial coherent state. To proceed, we first introduce our theoretical framework.

II. INTRAVALLEY SCATTERING: EXCITON RECOMBINATION

The exciton recombination is one important process leading to valley decoherence. Both the magnetic-field-induced valley Zeeman shift (Fig. 1) and the thermal (temperature)-effect-triggered band-gap (E_g) shrinking affect the exciton energy [23] and thus the exciton recombination rate. For the valley Zeeman shift, it comprises three distinct contributions from the spin, valley, and transition-metal atomic magnetic moments, while the magnetic response for the energy of *intravalley* excitons is fully attributed to the atomic contribution [24,25]. Among them, the valley magnetic moment does not affect the excitonic resonance of excitons within a given valley (i.e., intravalley exciton) that we consider, allowing us

*xsj@sdu.edu.cn

†yongjf@qfnu.edu.cn

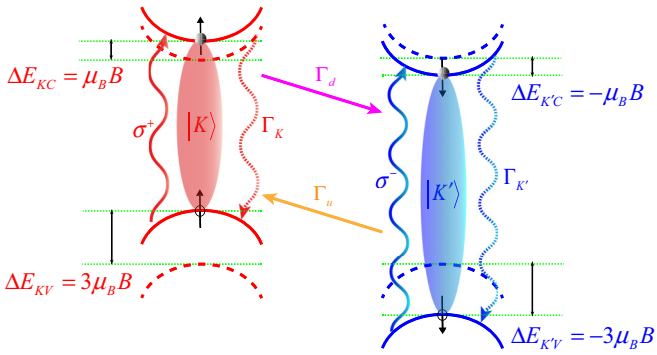

FIG. 1. Illustration of the spin-valley locked band structure in monolayer WS_2, with the magnetic field $B = 0$ (dashed curves) and $B > 0$ (solid curves). The red (blue) represents spin-up (spin-down) states in the K (K') valley, σ^+ (σ^-) denotes CP excitation, $\Delta E_{K(K')C(V)}$ stands for valley Zeeman shift for the conduction (valence) band, and $\Gamma_{K(K')}$ is the exciton recombination rate. The purple (orange) arrow denotes the intervalley scattering of excitons from a lower (higher) valley in energy to a higher (lower) one due to the e-h exchange and ex-ph interactions with the rate $\Gamma_{d(u)}$.

to ignore the valley contribution. For the conduction band, the atomic contribution (d_{z^2}) is zero, and thus only the spin magnetic moment matters with its contribution $\Delta_s^c = \mu_B B$, where μ_B is the Bohr magneton. Regarding the valence band, both atomic ($d_{x^2-y^2}$ and d_{xy}) and spin magnetic moments contribute to the valley Zeeman shifts, with contributions $\Delta_a^v = 2\mu_B B$ and $\Delta_s^v = \mu_B B$, respectively, leading to a total shift of $3\mu_B B$ (see Fig. 1). Note that for the bright exciton, this treatment of valley Zeeman shift with three contributions [24–27] is consistent with recent *ab initio* calculations, which deal with the valley (*intercellular*) and atomic (*intracellular*) contributions in a unified way associated with the orbital angular momentum [28–31]. However, when we consider dark excitonic states or deal with van der Waals heterostructures of TMDCs, it is better to resort to more rigorous consideration, treating the valley and atomic contributions in a unified way [28]. Regarding the thermal effect, which causes a reduction of E_g primarily due to the electron-phonon interaction [23], we adopt a fit with the Varshni equation $\Delta E_g = \alpha T^2/(T+\beta)$ [32], with T the temperature, $\alpha \approx 4.45 \times 10^{-4}$ eV/K a material relevant constant [23], and $\beta \approx 247.5$ K related to the Debye temperature [33]. Then the exciton energy reads $E_\xi = E_g - E_b + \lambda_c/2 - \lambda_v/2 - 2\xi\mu_B B$ [16], with E_b the exciton binding energy, $\lambda_{c(v)}$ the spin-orbit splitting in the conduction (valence) band, and $\xi = \pm 1$ the valley indices K and K'. Note that the last term in E_ξ describes the valley Zeeman shift. With all these considerations, the exciton recombination time is $\tau_\xi(T) = 1/\Gamma_\xi(T) = (3Mc^2 k_B T/2E_\xi^2)\tau(0)$ [34], with $\tau(0) = 0.19$ ps the recombination time near $T = 0$ [34], M the exciton mass, and c the speed of light.

III. INTERVALLEY SCATTERING: e-h EXCHANGE AND ex-ph INTERACTIONS

The e-h exchange and ex-ph interactions in general dominate intervalley scatterings, providing a unique channel for transfer of excitons from one valley to the other [35–42]. For the e-h exchange interaction, its magnitude essentially scales linearly with the center-of-mass wave vector $\mathbf{k}$ of excitons, and its direction depends on the orientation of $\mathbf{k}$ [43–45]; hence it provides an *effective* in-plane magnetic field driving the precession of valley pseudospin with different frequencies [46–48]. Due to various scatterings, e.g., with phonons, other excitons and defects, the exchange interaction, which depends on $\mathbf{k}$, may become random [49]. This is similar to the D'ykonov-Perel (DP) spin relaxation [50–52], induced by the momentum-dependent spin-orbit field, for two-dimensional electron gases in the diffusive regime. The incoherent intervalley transfer caused by the random exchange interaction manifests as a statistical average scattering time τ_{v0}. Further, in the presence of external magnetic field, the expectation value of valley pseudospin depends on the combined contributions of the in-plane and out-of-plane components, indicating that the influences of exchange interaction can be effectively tuned by the valley Zeeman splitting $\Delta E = E_{K'} - E_K$ [43]. Thus the magnetic-field-mediated intervalley scattering rate reads $\Gamma_v = 1/\tau_{v0} \times F(\Delta E)$, where $F(\Delta E) = \Gamma^2/(\Gamma^2 + \Delta E^2)$ [35,36], with $\tau_{v0} = 50$ ps the zero-field scattering time and $\Gamma = 0.1$ meV the width parameter associated with exciton momentum relaxation time [35], i.e., $\Gamma = \hbar/\tau_p$. Note that the magnitude of magnetic field at which the e-h exchange interaction is suppressed can be estimated by analyzing the momentum relaxation time τ_p [53,54].

Regarding the ex-ph interaction, since the excitons in both K and K' valleys have zero center-of-mass momentum, two K-point phonons are needed to ensure the momentum conservation for the transfer process. In such a situation, the intervalley scattering rate is proportional to the phonon occupation number, i.e., $\Gamma_{ph} \propto \exp(-\langle\hbar\omega_{ph}\rangle/k_B T)$ [37], with $\langle\hbar\omega_{ph}\rangle = 12$ meV the acoustic phonon energy near the K point [37–41], closing to the acoustic phonon energy reported in TMDCs [33,37,55]. Further, to capture the *asymmetry* of the phonon-related relaxation process caused by the lifting of valley degeneracy due to B field, the intervalley scattering rates associated with ex-ph interaction are expressed as Miller form, with $\Gamma_H = \Gamma_{ph} = 1/50\,\text{ps}^{-1}$ and $\Gamma_L = \Gamma_{ph}\exp(-\Delta E/k_B T)$ [12,56–58]. This ensures that excitonic scatterings from the valley of higher energy to the one of lower energy require emission of an additional phonon (Γ_H), whereas absorption of a phonon occurs in the opposite process (Γ_L), which is mediated by the Boltzmann factor and reduced to Γ_H at $B = 0$ (symmetric intervalley scattering). Combining two-part contributions from e-h exchange and ex-ph interactions, the total intervalley scattering rates can be written as $\Gamma_{u,d} = \Gamma_v + \Gamma_{H,L}$.

IV. PURE DEPHASING OF VALLEY EXCITON: ADDITIONAL COHERENCE DECAY

In addition to the exciton recombination, pure dephasing is also a significant source of coherence loss. Considering the Maialle-Silva-Sham (MSS) mechanism, an in-depth understanding of processes responsible for valley pure dephasing is exchange interaction [17,59]. Further, optical two-dimensional coherent spectroscopy reveals another pure dephasing pathway by elevating temperature [17,60], which is analogous to the exciton dephasing in semiconductor

quantum wells caused by the acoustic phonon scattering [61]. Hence the pure dephasing rate is expressed as $\gamma = \gamma_0 + \gamma_{\rm eh}^0 F(\Delta E) + \gamma_{\rm ph}^0 T$, where γ_0 is the residual exciton dephasing rate in the absence of e-h exchange and ex-ph interactions [60]. $\gamma_{\rm eh}^0 = 2\,{\rm ps}^{-1}$ is the dephasing rate related to exchange interaction at zero extra field [17], and the factor $F(\Delta E)$ stands for the suppression by the magnetic field [35,36]. $\gamma_{\rm ph}^0 = 1/12\,{\rm ps}^{-1}/{\rm K}$ denotes the ex-ph coupling strength [60]. The values of these parameters can be further analyzed experimentally from the homogeneous linewidth [60,62]. We exhibit the numerical relationship between the rate $\gamma_{\rm eh}$ ($\gamma_{\rm ph}$) and the magnetic field (temperature), see Fig. S1 [63] in the Supplemental Material [63]. When $B > 5\,{\rm T}$, the exchange interaction is completely suppressed by the vertical magnetic field so that the pure dephasing rate $\gamma_{\rm eh}$ trends to zero. In contrast, the rate $\gamma_{\rm ph}$ increases linearly with elevated temperature, which highlights the decisive role of phonon scattering at high temperatures.

V. VALLEY DYNAMICAL EVOLUTION: MASTER EQUATION

We incorporate the intra- and intervalley scatterings into the master equation of Lindblad form and employ the density matrix to illustrate evolutions of the valley coherence and exciton population. We adopt the basis set $\{|K\rangle, |K'\rangle, |0\rangle\}$ characterizing the exciton states in the K ($|K\rangle$) and K' ($|K'\rangle$) valleys and the ground state ($|0\rangle$). Also, note that the intervalley transfer of excitons is a process of *balancing* populations between the two valleys, which is described by two incoherent rate equations [19] (see Eq. (S5) [63]), while the exciton recombination refers to a one-way flow of valley information to the environment [64,65]. Then the Hamiltonian of the overall system reads $H = H_0 + H_{\rm E} + H_{\rm I}$, comprising contributions from the valley exciton (H_0) [15], environment ($H_{\rm E}$), and the interaction between valley and environment ($H_{\rm I}$):

$$\begin{aligned} H_0 &= \sum_{\xi} E_\xi c_\xi^\dagger c_\xi,\ \xi = K, K', \\ H_{\rm E} &= \hbar(\omega_L a_L^\dagger a_L + \omega_R a_R^\dagger a_R), \\ H_{\rm I} &= g_K \sigma_{K-} a_R^\dagger + g_{K'} \sigma_{K'-} a_L^\dagger + {\rm H.c.}, \end{aligned} \tag{1}$$

where $c_\xi^\dagger (c_\xi)$ stands for the exciton creation (annihilation) operator of the ξ ($= K, K'$) valley. $a_L^\dagger (a_L)$ and $a_R^\dagger (a_R)$ denote the creation (annihilation) operators of the left (L) and right (R) circularly polarized photons with the characteristic frequencies ω_L and ω_R. Constant g_ξ is the coupling strength between the exciton in the ξ valley with the corresponding circularly photon mode. Also, we have defined $\sigma_{\xi-} = |0\rangle\langle\xi|$ as the lowering operator, and H.c. denotes the Hermitian conjugate, indicating the exciton recombinations are from individual K and K' valleys, with emitting right and left circularly polarized photons, respectively. Thus the dynamical evolution of exciton valley coherence is described as

$$\frac{d}{dt}\rho_t = L(\rho_t) = L_0(\rho_t) + L_{\rm f}(\rho_t) + L_{\rm r}(\rho_t) + L_{\rm p}(\rho_t), \tag{2}$$

where $L_0(\rho_t)$ denotes the unitary evolution determined by the exciton Hamiltonian H_0, and $L_{\rm f}(\rho_t)$ means the exciton intervalley transfer between two valleys. $L_{\rm r}(\rho_t)$ [$L_{\rm p}(\rho_t)$] describes the exciton recombination (pure dephasing) process, referring to the rate Γ_ξ (γ) [66]. For more details about the operator $L(\rho_t)$, see the SM, Sec. I [63]. As the valley coherence strongly depends on the remnant excitonic populations, we define the coherence intensity characterizing the degree of valley coherence by employing the l_1-norm-based coherence measure [67,68], which in the basis set of $\rho_t = (\rho^K, \rho^{K'}, \rho^{K'K}, \rho^{KK'}, \rho_0)^T$ reads

$$C(\rho) = \sum_{i \neq j} |\rho^{ij}| = |\rho^{KK'}| + |\rho^{K'K}|, \tag{3}$$

with $0 \leqslant C(\rho) \leqslant 1$. And the coherence time τ_C can be defined as a time over which $C(\rho)$ essentially vanishes [69], characterizing the duration of coherence.

VI. TIME EVOLUTIONS OF DENSITY MATRIX ELEMENTS

For better understanding valley dynamics, we first look into how the exciton populations represented by the density matrix elements $\rho^{K(K')}$ and $\rho_0^{K(K')}$ evolve with time in the presence of both intra- and intervalley scatterings (Fig. 2). We focus on optical pumping of both CP and LP excitations, which gives rise to the *initial* states of $|\psi_0\rangle = |K\rangle$ (e.g., for σ^+ excitation) and $|\psi_0\rangle = 1/\sqrt{2}(|K\rangle + |K'\rangle)$, respectively, as a result of the valley selective transition rule. For the CP excitation (left panels in Fig. 2), as the excitons are initially generated in the K valley with $|\psi_0\rangle = |K\rangle$, we find that $\rho^{K'}$ first increases and then decreases after attaining its maximal value due to a combined effect of *intervalley* excitonic transfer and *intravalley* exciton recombination, in contrast to ρ^K, which consistently decreases, cf. ρ^K and $\rho^{K'}$ in Fig. 2(a). Now we examine the effect of temperature and magnetic field, both of which are found playing an important role in valley dynamics. As temperature increases, on the one hand, the process of exciton recombination is quenched, giving rise to considerable increment of $\tau_{K(K')}$; on the other hand, phonon-assisted intervalley scattering becomes more pronounced, leading to more balanced populations between K and K' valleys, cf. Figs. 2(a) and 2(c). As opposed to $\rho^{K,K'}$, $\rho_0^{K,K'}$ describing the population of recombined excitons consistently increases with time, as is expected. The B field lifts the valley degeneracy and introduces the asymmetry of intervalley scatterings (i.e., unbalanced Γ_H and Γ_L), thus refraining the exciton transfer from the K to K' valleys, resulting in an overall reduction of exciton population in the K' valley, cf. Figs. 2(a) and 2(e).

As for the LP excitation (right panels in Fig. 2), because of an *initial* coherent superposition of excitonic states in the two valleys with the same population, the dynamical evolution of ρ^K and $\rho^{K'}$ perfectly matches at zero B field, independent of temperature; see Figs. 2(b) and 2(d) for $T = 50$ and 300 K, respectively. Similarly, the populations for recombined excitons between the K and K' valleys are also locked to be equal as time evolves, cf. ρ_0^K and $\rho_0^{K'}$, though $\rho^{K(K')}$ and $\rho_0^{K(K')}$ exhibit opposite dynamic behavior. Further, even with the presence of valley Zeeman splitting, the distinction of excitonic populations between the two valleys is also greatly

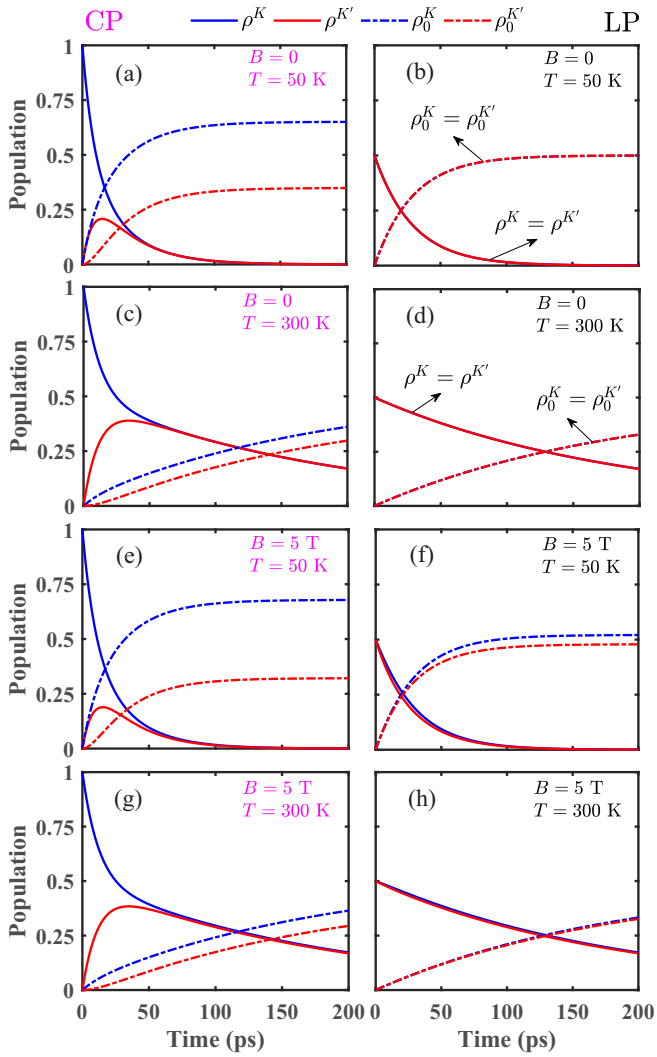

FIG. 2. Time evolutions of exciton populations for different magnetic fields and temperatures in the cases of CP (left panels) and LP (right panels) excitations. The density matrix element ρ^K ($\rho^{K'}$) stands for the remnant exciton population after recombination in the K (K') valleys, while ρ_0^K ($\rho_0^{K'}$) refers to the population of exciton undergoing recombination.

quenched [Figs. 2(f) and 2(h)], as compared to the case of CP excitation, cf. left and right panels.

These dynamical features of density matrix elements are helpful in understanding valley dynamics. For further illustrating the coherence behaviors, below we focus on the LP excitation, which is widely employed in experiments for coherent valley control [20,21].

VII. LP EXCITATION: MAGNETIC-FIELD-ENHANCED COHERENCE

The main channels leading to the decay of valley coherence comprises the intravalley exciton recombination ($\Gamma_{K(K')}$) and the pure dephasing process (γ). The former results in reduction of excitonic populations (Fig. 2), and the latter mainly

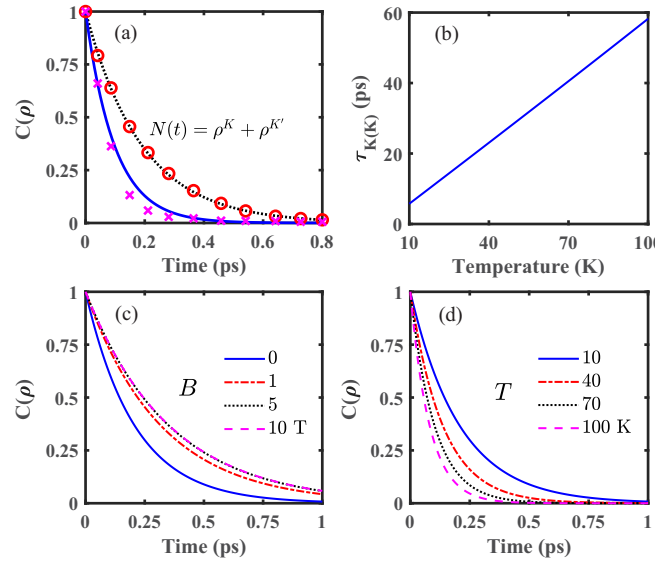

FIG. 3. (a) Time evolution of valley coherence (solid line, blue) and remnant exciton population (dashed line. black). The markers (crosses and circles) refer to the corresponding experimental data of Ref. [17]. (b) The exciton recombination lifetime as function of temperature [34,71]. (c),(d) Valley coherence dynamics at different magnetic fields ($T = 10$ K) (c) and temperatures ($B = 0$) (d).

originates from the e-h exchange and ex-ph interactions. For verifying the accuracy of our model, we first adopt experimental parameters in the work by Hao *et al.* [17], where the decoherence rate $\gamma_v = \Gamma_K + \gamma = 10.2\,\mathrm{ps}^{-1}$ with $\Gamma_K = 5.26$ and $\gamma = 4.94\,\mathrm{ps}^{-1}$ [17,60]. We reveal that the remnant exciton population, $N = \rho^K + \rho^{K'}$, tends to vanish at around 800 fs [dotted line in Fig. 3(a)], while the coherence time τ_C attains about 400 fs [solid line in Fig. 3(a)], in great agreement with experimental data [markers in Fig. 3(a)]. It is noteworthy that experimental reports of exciton lifetime in monolayer WS_2 usually ranges from tens to even hundreds of picoseconds [70–74]. Considering that the relaxation of excitonic population may provide an upper bound for valley coherence, below we consider the exciton lifetime ranging from 5 to 60 ps as the temperature varies from 10 to 100 K [Fig. 3(b)] [34,71], to explore a potential means of enhancing valley coherence. We first examine the magnetic response of valley coherence dynamics [Fig. 3(c)]. It is found that the maximal coherence intensity occurs *initially*, following that the initial state itself being a coherent superposition of valley excitons. Notably, when $B < 5$ T, we reveal magnetic-field-bolstered valley coherence in both its intensity and time, which arises from the quenching of the pure dephasing channel induced by the e-h exchange interaction as a result of lifting of valley degeneracy in the presence of B field. However, for $B > 5$ T we observe that the coherence dynamics starts to remain essentially unaltered as B varies, cf. dynamics behaviors at $B = 5$ and 10 T. This is because the pure dephasing induced by e-h exchange interaction becomes entirely suppressed at $B = 5$ T (see Fig. S1(a) [63]), and the other decoherence channels are basically unaffected by the B field. Note that the coherence time at $T = 10$ K even attains

$\tau_C \sim 1$ ps, facilitating complete control of qubits based on the valley pseudospin.

Now we turn to the temperature-related thermal effects, which essentially have two *compensating* consequences on valley coherence. On the one hand, the ex-ph interaction becomes more pronounced at escalated temperature, in favor of decay of coherence; on the other hand, a higher temperature implies a longer exciton recombination time, thus suppressing the valley decoherence. However, the *overall* effect is that the ex-ph interaction with increasing temperature gradually dominates over the other decoherence channels due to, i.e., the e-h exchange interaction or the exciton recombination [cf. Fig. S1(b) [63] and Fig. 3(b)]. Thus a shrinking of valley coherence at escalated temperature follows [Fig. 3(d)].

Despite the detrimental effect of temperature on valley coherence, we should emphasize the suppression of e-h exchange interaction by magnetic field provides a reliable route to enhance coherence intensity and enlarge the coherence time in a temperature range of $T = 10$–120 K. Also, the robustness of the coherence against B field when $B > 5$ T [Fig. 3(c)] also holds in a broad temperature range (see Fig. S2 [63]), facilitating coherent manipulation of the valley pseudospin. For practical application, a possible means of boosting coherence generation is to resort to the exciton-cavity coupling [19], which may open an additional channel of coherence transfer from photons to valley excitons.

VIII. EMERGING VALLEY COHERENCE OF DARK EXCITONS: WITH NO INITIAL COHERENCE

Under σ^+ CP excitation, only excitons in the K valley are generated, and thus there is no initial coherence. In this case the incoherent intervalley transfer prevents exciton dynamics from producing valley coherence. In contrast, for dark excitons the exchange interaction is a short-range local field effect; thus it weakly depends on center-of-mass momentum and can be treated as a constant with definite phase. In the basis $\{|K_d\rangle, |K'_d\rangle\}$, the system Hamiltonian of dark exciton has the form [15]

$$H_0^d = \begin{pmatrix} E_K^d + \delta & \delta \\ \delta & E_{K'}^d + \delta \end{pmatrix}, \tag{4}$$

with E_ξ^d the dark exciton energy and δ the short-range exchange interaction [15,75] that *mixes* different valley states together. Also, the dark excitons have a longer recombination lifetime than bright state, due to the weak coupling with photons of out-of-plane linear polarization. These features underline a potential coherent control based on dark excitons, even without initial coherence, as we discuss next.

For completeness we consider two initial states of $|\psi_0^d\rangle = 1/\sqrt{2}(|K_d\rangle + |K'_d\rangle)$ (with initial coherence) and $|\psi_0^d\rangle = |K_d\rangle$ (without initial coherence). The relevant parameters adopted in the simulation are $\delta = 0.6$ meV [15,75], recombination lifetime $\tau_\xi^d = 110$ ps [75], and pure dephasing rate $\gamma^d = 2.6\ \mathrm{ps}^{-1}$ at $T = 10$ K, with the super/subscript d denoting the dark. For a detailed derivation of valley coherent dynamics of dark excitons, see the SM, Sec. III [63]. Figure 4(a) shows the magnetic response of coherence behaviors with initial coherence. In this case we find that despite the long recombination lifetime of dark exciton at low temperature, its coherent evolution essentially coincides with that of the bright state, cf. Figs. 3(c) and 4(a). This is because valley coherence mainly depends on the pure dephasing in the presence of an initial coherent state. In addition, a constant exchange interaction avoids triggering the MSS mechanism, which means that the B field has negligible impact on the pure dephasing path. Hence the coherence intensity and time of dark excitons are not sensitive to the B field [see Fig. 4(a)]. Regarding the case without initial coherence, it is shown that the valley coherence can be generated through the *mixture* of excitonic states of two valleys by exchange interaction [Fig. 4(b)]. In contrast to the case with initial coherence, this emerging coherence depends not only on the generation channel, but also on the decay channel (i.e., decoherence), thus leading to a long coherence time ($\tau_C^d \sim 15$ ps), though with quenched coherence intensity. Also, the *mixture* effect of exchange interaction can be tuned by the valley splitting, which manifests as a marked dependence of this emerging coherence on the B field.

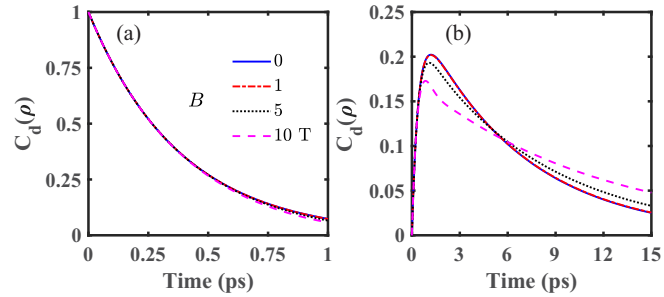

FIG. 4. Valley coherence dynamics of dark excitons at different magnetic fields ($T = 10$ K) for initial coherent state (a) and initial incoherent state (b).

We should emphasize that, in general, as dark excitons are generated by the intravalley scattering from bright excitons [15,16,58,76], a more precise description of coherent valley dynamics requires to take into account the bright and dark states simultaneously. In particular, when the magnetic field has an in-plane component, it even mixes the bright and dark states. More work is needed to explore these interesting possibilities.

IX. CONCLUSIONS

The artificial manipulation of valley pseudospin requires a sufficiently advanced coherence quality. We have developed a microscopic model in monolayer WS_2 involving both intra- and intervalley scatterings, and unveiled magnetically tunable exciton valley coherence mediated by the e-h exchange and ex-ph interactions. For the LP excitation, which is accompanied with an *initial* coherence, our determined valley dynamics manifests the coherence decay being faster than the exciton population relaxation and agrees with experimental data by Hao *et al.* [17]. Further, we find that magnetic field may quench the e-h exchange induced pure dephasing, allowing *magnetic* regulation of valley coherence. In particular, at low temperatures for which the ex-ph interaction is weak, the coherence time attains 1 ps, a significant improvement over previously reported values in the subpicosecond scale

[17,60,77]. For practical considerations, we should emphasize that the density of exciton gas may also affect the coherence dynamics. A higher density will enhance the strength of exchange interaction [49,60,78], which requires a stronger B field (>5 T) to suppress the pure dephasing path. Correspondingly, a higher B field is needed for the valley coherence to exhibit robustness. Additionally, the coherence time is expected to be further enlarged through external means, e.g., exciton-cavity coupling [19], electron doping [79], and enhanced dielectric screening [80]. For the dark excitons, we observe an emerging valley coherence even in the absence of an initial coherent state, and this emerging coherence has long coherence time ($\sim$15 ps), though with quenched coherence intensity. Our work provides an insight into *tunable* valley coherence and coherent valley control based on dark excitons.

ACKNOWLEDGMENTS

We thank Paulo E. Faria Jr. and Gerson J. Ferreira for valuable discussions. This work was supported by the National Natural Science Foundation of China (Nos. 11974212, 12274256, and 11874236) and the Major Basic Program of Natural Science Foundation of Shandong Province (Grant No. ZR2021ZD01).

[1] K. S. Novoselov, D. Jiang, F. Schedin, T. J. Booth, V. V. Khotkevich, S. V. Morozov, and A. K. Geim, Two-dimensional atomic crystals, Proc. Natl. Acad. Sci. USA **102**, 10451 (2005).

[2] D. Xiao, G.-B. Liu, W. Feng, X. Xu, and W. Yao, Coupled Spin and Valley Physics in Monolayers of MoS_2 and other Group-VI Dichalcogenides, Phys. Rev. Lett. **108**, 196802 (2012).

[3] C. Robert, D. Lagarde, F. Cadiz, G. Wang, B. Lassagne, T. Amand, A. Balocchi, P. Renucci, S. Tongay, B. Urbaszek, and X. Marie, Exciton radiative lifetime in transition metal dichalcogenide monolayers, Phys. Rev. B **93**, 205423 (2016).

[4] K. He, N. Kumar, L. Zhao, Z. Wang, K. F. Mak, H. Zhao, and J. Shan, Tightly Bound Excitons in Monolayer WSe_2, Phys. Rev. Lett. **113**, 026803 (2014).

[5] P. Dey, L. Yang, C. Robert, G. Wang, B. Urbaszek, X. Marie, and S. A. Crooker, Gate-Controlled Spin-Valley Locking of Resident Carriers in WSe_2 Monolayers, Phys. Rev. Lett. **119**, 137401 (2017).

[6] X. Xu, W. Yao, D. Xiao, and T. F. Heinz, Spin and pseudospins in layered transition metal dichalcogenides, Nat. Phys. **10**, 343 (2014).

[7] S. Mouri, Y. Miyauchi, M. Toh, W. Zhao, G. Eda, and K. Matsuda, Nonlinear photoluminescence in atomically thin layered WSe_2 arising from diffusion-assisted exciton-exciton annihilation, Phys. Rev. B **90**, 155449 (2014).

[8] M. M. Ugeda, A. J. Bradley, S.-F. Shi, F. H. Da Jornada, Y. Zhang, D. Y. Qiu, W. Ruan, S.-K. Mo, Z. Hussain, Z.-X. Shen, F. Wang, S. G. Louie, and M. F. Crommie, Giant bandgap renormalization and excitonic effects in a monolayer transition metal dichalcogenide semiconductor, Nat. Mater. **13**, 1091 (2014).

[9] Z. Ye, T. Cao, K. O'Brien, H. Zhu, X. Yin, Y. Wang, S. G. Louie, and X. Zhang, Probing excitonic dark states in single-layer tungsten disulphide, Nature (London) **513**, 214 (2014).

[10] A. Chernikov, T. C. Berkelbach, H. M. Hill, A. Rigosi, Y. Li, B. Aslan, D. R. Reichman, M. S. Hybertsen, and T. F. Heinz, Exciton Binding Energy and Nonhydrogenic Rydberg Series in Monolayer WS_2, Phys. Rev. Lett. **113**, 076802 (2014).

[11] J. Fu, A. Bezerra, and F. Qu, Valley dynamics of intravalley and intervalley multiexcitonic states in monolayer WS_2, Phys. Rev. B **97**, 115425 (2018).

[12] J. Fu, J. M. R. Cruz, and F. Qu, Valley dynamics of different trion species in monolayer WSe_2, Appl. Phys. Lett. **115**, 082101 (2019).

[13] G. Wang, M. M. Glazov, C. Robert, T. Amand, X. Marie, and B. Urbaszek, Double Resonant Raman Scattering and Valley Coherence Generation in Monolayer WSe_2, Phys. Rev. Lett. **115**, 117401 (2015).

[14] A. M. Jones, H. Yu, N. J. Ghimire, S. Wu, G. Aivazian, J. S. Ross, B. Zhao, J. Yan, D. G. Mandrus, D. Xiao *et al.*, Optical generation of excitonic valley coherence in monolayer WSe_2, Nat. Nanotechnol. **8**, 634 (2013).

[15] M. R. Molas, A. O. Slobodeniuk, T. Kazimierczuk, K. Nogajewski, M. Bartos, P. Kapuściński, K. Oreszczuk, K. Watanabe, T. Taniguchi, C. Faugeras, P. Kossacki, D. M. Basko, and M. Potemski, Probing and Manipulating Valley Coherence of Dark Excitons in Monolayer WSe_2, Phys. Rev. Lett. **123**, 096803 (2019).

[16] F. Qu, H. Bragança, R. Vasconcelos, F. Liu, S.-J. Xie, and H. Zeng, Controlling valley splitting and polarization of dark- and bi-excitons in monolayer WS_2 by a tilted magnetic field, 2D Mater. **6**, 045014 (2019).

[17] K. Hao, G. Moody, F. Wu, C. K. Dass, L. Xu, C.-H. Chen, L. Sun, M.-Y. Li, L.-J. Li, A. H. Macdonald *et al.*, Direct measurement of exciton valley coherence in monolayer WSe_2, Nat. Phys. **12**, 677 (2016).

[18] C. Rupprecht, E. Sedov, M. Klaas, H. Knopf, M. Blei, N. Lundt, S. Tongay, T. Taniguchi, K. Watanabe, U. Schulz, A. Kavokin, F. Eilenberger, S. Höfling, and C. Schneider, Manipulation of room-temperature valley-coherent exciton-polaritons in atomically thin crystals by real and artificial magnetic fields, 2D Mater. **7**, 035025 (2020).

[19] L. Qiu, C. Chakraborty, S. Dhara, and A. N. Vamivakas, Room-temperature valley coherence in a polaritonic system, Nat. Commun. **10**, 1513 (2019).

[20] G. Wang, X. Marie, B. L. Liu, T. Amand, C. Robert, F. Cadiz, P. Renucci, and B. Urbaszek, Control of Exciton Valley Coherence in Transition Metal Dichalcogenide Monolayers, Phys. Rev. Lett. **117**, 187401 (2016).

[21] R. Schmidt, A. Arora, G. Plechinger, P. Nagler, A. Granados del Águila, M. V. Ballottin, P. C. M. Christianen, S. Michaelis de Vasconcellos, C. Schüller, T. Korn, and R. Bratschitsch, Magnetic-Field-Induced Rotation of Polarized Light Emission from Monolayer WS_2, Phys. Rev. Lett. **117**, 077402 (2016).

[22] Z. Ye, D. Sun, and T. F. Heinz, Optical manipulation of valley pseudospin, Nat. Phys. **13**, 26 (2017).

[23] P. Nagler, M. V. Ballottin, A. A. Mitioglu, M. V. Durnev, T. Taniguchi, K. Watanabe, A. Chernikov, C. Schüller, M. M. Glazov, P. C. M. Christianen, and T. Korn, Zeeman Splitting

and Inverted Polarization of Biexciton Emission in Monolayer WS_2, Phys. Rev. Lett. **121**, 057402 (2018).

[24] M. Koperski, M. R. Molas, A. Arora, K. Nogajewski, M. Bartos, J. Wyzula, D. Vaclavkova, P. Kossacki, and M. Potemski, Orbital, spin and valley contributions to Zeeman splitting of excitonic resonances in $MoSe_2$, WSe_2, and WS_2 monolayers, 2D Mater. **6**, 015001 (2018).

[25] G. Aivazian, Z. Gong, A. M. Jones, R.-L. Chu, J. Yan, D. G. Mandrus, C. Zhang, D. Cobden, W. Yao, and X. Xu, Magnetic control of valley pseudospin in monolayer WSe_2, Nat. Phys. **11**, 148 (2015).

[26] R. Vasconcelos, H. Bragança, F. Qu, and J. Fu, Dark exciton brightening and its engaged valley dynamics in monolayer WSe_2, Phys. Rev. B **98**, 195302 (2018).

[27] M. Van der Donck, M. Zarenia, and F. M. Peeters, Strong valley Zeeman effect of dark excitons in monolayer transition metal dichalcogenides in a tilted magnetic field, Phys. Rev. B **97**, 081109(R) (2018).

[28] P. E. F. Junior, K. Zollner, T. Woźniak, M. Kurpas, M. Gmitra, and J. Fabian, First-principles insights into the spin-valley physics of strained transition metal dichalcogenides monolayers, New J. Phys. **24**, 083004 (2022).

[29] C. Robert, H. Dery, L. Ren, D. Van Tuan, E. Courtade, M. Yang, B. Urbaszek, D. Lagarde, K. Watanabe, T. Taniguchi, T. Amand, and X. Marie, Measurement of Conduction and Valence Bands *g*-Factors in a Transition Metal Dichalcogenide Monolayer, Phys. Rev. Lett. **126**, 067403 (2021).

[30] T. Deilmann, P. Krüger, and M. Rohlfing, Ab Initio Studies of Exciton *g* Factors: Monolayer Transition Metal Dichalcogenides in Magnetic Fields, Phys. Rev. Lett. **124**, 226402 (2020).

[31] T. Woźniak, P. E. Faria Junior, G. Seifert, A. Chaves, and J. Kunstmann, Exciton *g* factors of van der waals heterostructures from first-principles calculations, Phys. Rev. B **101**, 235408 (2020).

[32] Y. Varshni, Temperature dependence of the energy gap in semiconductors, Physica **34**, 149 (1967).

[33] S. Helmrich, R. Schneider, A. W. Achtstein, A. Arora, B. Herzog, S. M. de Vasconcellos, M. Kolarczik, O. Schöps, R. Bratschitsch, U. Woggon, and N. Owschimikow, Exciton–phonon coupling in mono- and bilayer $MoTe_2$, 2D Mater. **5**, 045007 (2018).

[34] M. Palummo, M. Bernardi, and J. C. Grossman, Exciton radiative lifetimes in two-dimensional transition metal dichalcogenides, Nano Lett. **15**, 2794 (2015).

[35] A. Surrente, u. Kłopotowski, N. Zhang, M. Baranowski, A. A. Mitioglu, M. V. Ballottin, P. C. Christianen, D. Dumcenco, Y.-C. Kung, D. K. Maude, A. Kis, and P. Plochocka, Intervalley scattering of interlayer excitons in a $MoS_2/MoSe_2/MoS_2$ heterostructure in high magnetic field, Nano Lett. **18**, 3994 (2018).

[36] D. S. Brandão, E. C. Castro, H. Zeng, J. Zhao, G. S. Diniz, J. Fu, A. L. A. Fonseca, C. A. N. Júnior, and F. Qu, Phonon-fostered valley polarization of interlayer excitons in van der Waals heterostructures, J. Phys. Chem. C **126**, 18128 (2022).

[37] H. Zeng, J. Dai, W. Yao, D. Xiao, and X. Cui, Valley polarization in MoS_2 monolayers by optical pumping, Nat. Nanotechnol. **7**, 490 (2012).

[38] X. Li, J. T. Mullen, Z. Jin, K. M. Borysenko, M. Buongiorno Nardelli, and K. W. Kim, Intrinsic electrical transport properties of monolayer silicene and MoS_2 from first principles, Phys. Rev. B **87**, 115418 (2013).

[39] S. Helmrich, K. Sampson, D. Huang, M. Selig, K. Hao, K. Tran, A. Achstein, C. Young, A. Knorr, E. Malic, U. Woggon, N. Owschimikow, and X. Li, Phonon-Assisted Intervalley Scattering Determines Ultrafast Exciton Dynamics in $MoSe_2$ Bilayers, Phys. Rev. Lett. **127**, 157403 (2021).

[40] G. Kioseoglou, A. T. Hanbicki, M. Currie, A. L. Friedman, and B. T. Jonker, Optical polarization and intervalley scattering in single layers of MoS_2 and $MoSe_2$, Sci. Rep. **6**, 25041 (2016).

[41] B. R. Carvalho, Y. Wang, S. Mignuzzi, D. Roy, M. Terrones, C. Fantini, V. H. Crespi, L. M. Malard, and M. A. Pimenta, Intervalley scattering by acoustic phonons in two-dimensional MoS_2 revealed by double-resonance Raman spectroscopy, Nat. Commun. **8**, 14670 (2017).

[42] S. M. Sadeghi and J. Z. Wu, Gain without inversion and enhancement of refractive index via intervalley quantum coherence transfer in hybrid WS_2-metallic nanoantenna systems, Phys. Rev. A **103**, 043713 (2021).

[43] H. S. Borges, C. A. N. Júnior, D. S. Brandão, F. Liu, V. V. R. Pereira, S. J. Xie, F. Qu, and A. M. Alcalde, Persistent entanglement of valley exciton qubits in transition metal dichalcogenides integrated into a bimodal optical cavity, Phys. Rev. B **107**, 035404 (2023).

[44] S.-Y. Chen, T. Goldstein, J. Tong, T. Taniguchi, K. Watanabe, and J. Yan, Superior Valley Polarization and Coherence of 2*s* Excitons in Monolayer WSe_2, Phys. Rev. Lett. **120**, 046402 (2018).

[45] G. Moody, K. Tran, X. Lu, T. Autry, J. M. Fraser, R. P. Mirin, L. Yang, X. Li, and K. L. Silverman, Microsecond Valley Lifetime of Defect-Bound Excitons in Monolayer WSe_2, Phys. Rev. Lett. **121**, 057403 (2018).

[46] C. A. Jiménez-Orjuela, H. Vinck-Posada, and J. M. Villas-Bôas, Dark excitons in a quantum-dot–cavity system under a tilted magnetic field, Phys. Rev. B **96**, 125303 (2017).

[47] Y.-C. Wu, T. Taniguchi, K. Watanabe, and J. Yan, Enhancement of exciton valley polarization in monolayer MoS_2 induced by scattering, Phys. Rev. B **104**, L121408 (2021).

[48] T. Yu and M. W. Wu, Valley depolarization due to intervalley and intravalley electron-hole exchange interactions in monolayer MoS_2, Phys. Rev. B **89**, 205303 (2014).

[49] F. Mahmood, Z. Alpichshev, Y.-H. Lee, J. Kong, and N. Gedik, Observation of exciton-exciton interaction mediated valley depolarization in monolayer $MoSe_2$, Nano Lett. **18**, 223 (2018).

[50] J. Fabian, A. Matos-Abiague, C. Ertler, P. Stano, and I. Žutić, Semiconductor spintronics, Acta Phys. Slovaca **57**, (2007).

[51] K. Shen, R. Raimondi, and G. Vignale, Theory of coupled spin-charge transport due to spin-orbit interaction in inhomogeneous two-dimensional electron liquids, Phys. Rev. B **90**, 245302 (2014).

[52] I. R. de Assis, R. Raimondi, and G. J. Ferreira, Spin drift-diffusion for two-subband quantum wells, Phys. Rev. B **103**, 165304 (2021).

[53] E. Blackwood, M. J. Snelling, R. T. Harley, S. R. Andrews, and C. T. B. Foxon, Exchange interaction of excitons in GaAs heterostructures, Phys. Rev. B **50**, 14246 (1994).

[54] M. Z. Maialle, E. A. de Andrada e Silva, and L. J. Sham, Exciton spin dynamics in quantum wells, Phys. Rev. B **47**, 15776 (1993).

[55] S. Jiménez Sandoval, D. Yang, R. F. Frindt, and J. C. Irwin, Raman study and lattice dynamics of single molecular layers of MoS_2, Phys. Rev. B **44**, 3955 (1991).

[56] A. Miller and E. Abrahams, Impurity conduction at low concentrations, Phys. Rev. **120**, 745 (1960).

[57] A. Dash, D. Scheunemann, and M. Kemerink, Comprehensive Model for the Thermoelectric Properties of Two-Dimensional Carbon Nanotube Networks, Phys. Rev. Applied **18**, 064022 (2022).

[58] M. Baranowski, A. Surrente, D. K. Maude, M. Ballottin, A. A. Mitioglu, P. C. M. Christianen, Y. C. Kung, D. Dumcenco, A. Kis, and P. Plochocka, Dark excitons and the elusive valley polarization in transition metal dichalcogenides, 2D Mater. **4**, 025016 (2017).

[59] A. Vinattieri, J. Shah, T. C. Damen, D. S. Kim, L. N. Pfeiffer, M. Z. Maialle, and L. J. Sham, Exciton dynamics in GaAs quantum wells under resonant excitation, Phys. Rev. B **50**, 10868 (1994).

[60] G. Moody, C. Kavir Dass, K. Hao, C.-H. Chen, L.-J. Li, A. Singh, K. Tran, G. Clark, X. Xu, G. Berghäuser, E. Malic, A. Knorr, and X. Li, Intrinsic homogeneous linewidth and broadening mechanisms of excitons in monolayer transition metal dichalcogenides, Nat. Commun. **6**, 8315 (2015).

[61] L. Schultheis, A. Honold, J. Kuhl, K. Köhler, and C. W. Tu, Optical dephasing of homogeneously broadened two-dimensional exciton transitions in GaAs quantum wells, Phys. Rev. B **34**, 9027 (1986).

[62] M. Selig, G. Berghäuser, A. Raja, P. Nagler, C. Schüller, T. F. Heinz, T. Korn, A. Chernikov, E. Malic, and A. Knorr, Excitonic linewidth and coherence lifetime in monolayer transition metal dichalcogenides, Nat. Commun. **7**, 13279 (2016).

[63] See Supplemental Material at http://link.aps.org/supplemental/10.1103/PhysRevB.108.035419 for the derivation of the valley density matrix for bright excitons and of the valley coherent dynamics for dark excitons. It also contains Refs. [62, 65–67].

[64] H.-P. Breuer, E.-M. Laine, and J. Piilo, Measure for the Degree of Non-Markovian Behavior of Quantum Processes in Open Systems, Phys. Rev. Lett. **103**, 210401 (2009).

[65] K. Lan, Q. Du, L. Kang, X. Tang, L. Jiang, Y. Zhang, and X. Cai, Dynamics of an open double quantum dot system via quantum measurement, Phys. Rev. B **101**, 174302 (2020).

[66] P. Rebentrost, M. Mohseni, I. Kassal, S. Lloyd, and A. Aspuru-Guzik, Environment-assisted quantum transport, New J. Phys. **11**, 033003 (2009).

[67] K. Lan, S. Xie, and X. Cai, Geometric quantum speed limits for Markovian dynamics in open quantum systems, New J. Phys. **24**, 055003 (2022).

[68] T. Baumgratz, M. Cramer, and M. B. Plenio, Quantifying Coherence, Phys. Rev. Lett. **113**, 140401 (2014).

[69] The coherence time is also widely defined as a time over which the coherence intensity decays to e^{-1} of its initial value.

[70] G. Wang, L. Bouet, D. Lagarde, M. Vidal, A. Balocchi, T. Amand, X. Marie, and B. Urbaszek, Valley dynamics probed through charged and neutral exciton emission in monolayer WSe_2, Phys. Rev. B **90**, 075413 (2014).

[71] L. Yuan and L. Huang, Exciton dynamics and annihilation in WS_2 2D semiconductors, Nanoscale **7**, 7402 (2015).

[72] D. Lagarde, L. Bouet, X. Marie, C. R. Zhu, B. L. Liu, T. Amand, P. H. Tan, and B. Urbaszek, Carrier and Polarization Dynamics in Monolayer MoS_2, Phys. Rev. Lett. **112**, 047401 (2014).

[73] H. Liu, C. Wang, Z. Zuo, D. Liu, and J. Luo, Direct visualization of exciton transport in defective few-layer WS_2 by ultrafast microscopy, Adv. Mater. **32**, 1906540 (2020).

[74] H. H. Fang, B. Han, C. Robert, M. A. Semina, D. Lagarde, E. Courtade, T. Taniguchi, K. Watanabe, T. Amand, B. Urbaszek, M. M. Glazov, and X. Marie, Control of the Exciton Radiative Lifetime in van der Waals Heterostructures, Phys. Rev. Lett. **123**, 067401 (2019).

[75] C. Robert, T. Amand, F. Cadiz, D. Lagarde, E. Courtade, M. Manca, T. Taniguchi, K. Watanabe, B. Urbaszek, and X. Marie, Fine structure and lifetime of dark excitons in transition metal dichalcogenide monolayers, Phys. Rev. B **96**, 155423 (2017).

[76] O. Abdurazakov, C. Li, and Y.-P. Shim, Formation of dark excitons in monolayer transition metal dichalcogenides by a vortex beam: Optical selection rules, arXiv:2212.13240 (2022).

[77] P. Dey, J. Paul, Z. Wang, C. E. Stevens, C. Liu, A. H. Romero, J. Shan, D. J. Hilton, and D. Karaiskaj, Optical Coherence in Atomic-Monolayer Transition-Metal Dichalcogenides Limited by Electron-Phonon Interactions, Phys. Rev. Lett. **116**, 127402 (2016).

[78] D. Erkensten, S. Brem, and E. Malic, Exciton-exciton interaction in transition metal dichalcogenide monolayers and van der Waals heterostructures, Phys. Rev. B **103**, 045426 (2021).

[79] L. Yang, N. A. Sinitsyn, W. Chen, J. Yuan, J. Zhang, J. Lou, and Scott, Long-lived nanosecond spin relaxation and spin coherence of electrons in monolayer MoS_2 and WS_2, Nat. Phys. **11**, 830 (2015).

[80] G. Gupta, K. Watanabe, T. Taniguchi, and K. Majumdar, Observation of ∼100% valley-coherent excitons in monolayer MoS_2 through giant enhancement of valley coherence time, Light-Sci. Appl. **12**, 173 (2023).